DENTAL MATERIALS 33 (2017) 84–98

Available online at www.sciencedirect.com

ScienceDirect

journal homepage: www.intl.elsevierhealth.com/journals/dema

Chairside CAD/CAM materials. Part 1: Measurement of elastic constants and microstructural characterization

Renan Belli[a], *Michael Wendler*[a,b], *Dominique de Ligny*[c], *Maria Rita Cicconi*[c], *Anselm Petschelt*[a], *Herwig Peterlik*[d], *Ulrich Lohbauer*[a,*]

[a] *Friedrich-Alexander Universität Erlangen-Nürnberg (FAU), Zahnklinik 1 — Zahnerhaltung und Parodontologie, Forschungslabor für dentale Biomaterialien, Glueckstrasse 11, 91054 Erlangen, Germany*

[b] *Department of Restorative Dentistry, Faculty of Dentistry, University of Concepción, Concepción, Chile*

[c] *Department of Glass and Ceramics, Institute of Materials Science, Friedrich-Alexander University of Erlangen-Nuremberg, Martenstrasse 5, Erlangen, Germany*

[d] *Faculty of Physics, University of Vienna, Boltzmanngasse 5, A-1090 Vienna, Austria*

ARTICLE INFO

Article history:
Received 24 October 2016
Accepted 26 October 2016

Keywords:
Ceramic
Resin composite
CAD/CAM
Chairside
Elastic modulus
Poisson's ratio
Microstructure

ABSTRACT

Objective. A deeper understanding of the mechanical behavior of dental restorative materials requires an insight into the materials elastic constants and microstructure. Here we aim to use complementary methodologies to thoroughly characterize chairside CAD/CAM materials and discuss the benefits and limitations of different analytical strategies.

Methods. Eight commercial CAM/CAM materials, ranging from polycrystalline zirconia (e.max ZirCAD, Ivoclar-Vivadent), reinforced glasses (Vitablocs Mark II, VITA; Empress CAD, Ivoclar-Vivadent) and glass-ceramics (e.max CAD, Ivoclar-Vivadent; Suprinity, VITA; Celtra Duo, Dentsply) to hybrid materials (Enamic, VITA; Lava Ultimate, 3M ESPE) have been selected. Elastic constants were evaluated using three methods: Resonant Ultrasound Spectroscopy (RUS), Resonant Beam Technique (RBT) and Ultrasonic Pulse-Echo (PE). The microstructures were characterized using Scanning Electron Microscopy (SEM), Energy Dispersive X-ray Spectroscopy (EDX), Raman Spectroscopy and X-ray Diffraction (XRD).

Results. Young's modulus (E), Shear modulus (G), Bulk modulus (B) and Poisson's ratio (ν) were obtained for each material. E and ν reached values ranging from 10.9 (Lava Ultimate) to 201.4 (e.max ZirCAD) and 0.173 (Empress CAD) to 0.47 (Lava Ultimate), respectively. RUS showed to be the most complex and reliable method, while the PE method the easiest to perform but most unreliable. All dynamic methods have shown limitations in measuring the elastic constants of materials showing high damping behavior (hybrid materials). SEM images, Raman spectra and XRD patterns were made available for each material, showing to be complementary tools in the characterization of their crystal phases.

* *Corresponding author at*: Research Laboratory for Dental Biomaterials, Dental Clinic 1 — Operative Dentistry and Periodontology, Glueckstrasse 11, D-91054 Erlangen, Germany. Fax: +49 9131 853 3603.
E-mail address: ulrich.lohbauer@fau.de (U. Lohbauer).

http://dx.doi.org/10.1016/j.dental.2016.10.009

Significance. Here different methodologies are compared for the measurement of elastic constants and microstructural characterization of CAD/CAM restorative materials. The elastic properties and crystal phases of eight materials are herein fully characterized.

1. Introduction

Dental aesthetic indirect restoratives, formally supplied mainly as powders (glassy veneers) or pastes (resin composites), now find their way to the user in a ready-to-use pre-processed state, whether in block (cuboid) or blank (disc) geometries. The change in the form in which restorative materials were made available for processing constituted nothing but a natural – and inevitable – step ensuing from the development and establishment of CAD/CAM technology in dentistry. Most materials are now fully produced in an ideal industrial environment, ensuring quality standards hardly achieved under laboratorial/clinical conditions. Their processing diverges from traditional additive techniques, in that blocks and blanks are machined down to the final shape using the subtractive route. This concept allowed the unprecedent application of densely sintered high-strength glass-free polycrystalline ceramics in dentistry, such as zirconium dioxide (ZrO_2), aluminum oxide (Al_2O_3) and their composites, whose powders are isostatically pressed in block/blank form and pre-sintered prior to machining (green bodies). Some monolithic glassy products are also offered in a meta-sintered stage to facilitate grinding, and the later piece is subjected to a final crystallization firing, such as with lithium disilicate (LS_2) and lithium silicate (LS) glass-ceramics.

Although easier for users, the form in which materials are now delivered pose new challenges for those who test them (i.e., scientists and manufacturers looking for quality control). Especially for small partial- and single-unit restorations, CAD/CAM material blocks come only in diminute blocks of approximately 18 mm × 16 mm × 18 mm^3 (e.g., C16 blocks) or smaller (e.g., C14, I12, I10, etc.). From such block sizes test specimens cannot be produced in common beam geometries recommended by appropriate testing standards for the measurement of typical mechanical properties. To name a few examples, the European standard EN 843-1 for testing the uniaxial flexural strength of ceramics in four-point bending recommends a minimum outer span length of 20 mm [1], as does ASTM C 1161 for advanced ceramics [2], a condition that requires specimens of at least 22 mm in length. Many other national and international standards for strength testing of ceramics impose similar restrictions. For polymerizable resin composites the dental standard ISO 4049 advocates 25 mm-long specimens for a 20 mm span length in the three-point bending set-up [3]. Most standards standardizing the test of fracture toughness in bending, such as [4–8], also advocate span lengths between 20 and 40 mm. Some controversial exceptions exist, such as ISO 6872 for dental ceramics, allowing spans of 12 mm for three-point bending and 16 mm for four-point bending strength testing [9]. Although feasible, the miniaturization of bending tests come with wider error margins in tow [10,11], requiring custom fixtures of increased sophistication and extra caution in specimen preparation and testing [12]. The technique sensitivity involved in miniaturized set-ups is not addressed in ISO 6872, a standard broadly used by manufacturers for testing and advertising new products due to its flexible dimension requirements. Alternatively to uniaxial tests using bars, reduced specimen dimensions can be prepared out of small CAD/CAM blocks and tested in biaxial flexure, using set-ups like the piston-on-ring, ring-on-ring, piston-on-three-balls, and many other variations. These configurations use a disc-shaped geometry due to its rotational symmetry, which requires grinding of cuboid blocks into cylinders before sectioning them in discs, an inconvenient step for ordinary labs.

Set out to facilitate the mechanical testing of dental restorative materials available as CAD/CAM blocks, the authors devised a series of contributions aimed to introduce to the dental materials field the test method of biaxial flexural strength based on the ball-on-three-balls set-up developed by Börger et al. [13–15]. The test is scalable for small specimen sizes [16,17], adaptable for rectangular plate geometries [18], and intended also for fracture toughness testing [19,20]. The stresses in discs and plates using the ball-on-three-balls test is biaxial in nature, requiring the knowledge of the material's elastic constants (i.e., Poisson's ratio and Young's modulus) as parameters for the numerical solutions. The Poisson's ratio (ν) is a fundamental parameter in biaxial stress state problems by means of the biaxial (or effective) Elastic modulus (E), expressed as $E' = E/(1-\nu)$, even though the importance of accurate measurements of ν are not always appreciated. For example, again in ISO 6872, ν is required in the analytical solution for the pinston-on-three-balls biaxial flexural strength test, but the standard lets off easy, suggesting: "*If the value for the ceramic concerned is not known, use Poisson's ratio = 0.25*" [9]. This obviously leads to errors in strength determination using the solution given therein, from ~0.67% for a variation in ν of 0.01, up to ~3.38% for an error of ±0.05 in the value for ν. As will be shown later, the Poisson's ratio of most dental ceramics varies between 0.20 and 0.25. A disregard of material specific Poisson's ratio has also been shown to result in inaccuracies in determining the fracture toughness of ceramic materials using the surface crack in flexure method by means of erroneous estimations of the crack geometry factor, Y. The classical Newman and Raju formula is used to derive Y for a general case of $\nu = 0.3$, leading to errors up to 40% in extreme cases, according to a recent analysis by Strobl et al. [21] (in general the Newman and Raju solution for Y results in an overestimation of K_{Ic} by 8–10% [own observations]). Clearly there is no place for approximations, as often perpetrated in the dental literature, and accurate measurements of elastic constants are mandatory prior to any mechanical testing.

Elastic properties are mainly dictated by the microstructure and material composition. Unfortunately, information provided by the manufacturers are often incomplete or labeled with misleading terminologies regarding phase constituents. Terms like "Polymer-infiltrated Ceramic Network", "Resin Nano-Ceramic" or "Zirconia-reinforced Lithium Silicate Ceramic" have been used to advertise recent CAD/CAM restoratives, but deeper microstructural analyses performed by independent scientific peers are generally missing.

The present study focuses on the methodological aspects of the determination of elastic constants in dental materials supplied as CAD/CAM chairside blocks. Materials of different classes were selected, and a thorough microstructural/phase characterization was conducted using Scanning Electron Microscopy (SEM), Energy Dispersive X-ray Spectroscopy (EDX), Raman Spectroscopy and X-ray Diffraction (XRD). Structure-property relationships are ultimately discussed within the frame of phase constituents and elastic constants for different restorative classes.

2. Background

2.1. Elastic constants

Materials under mechanical stress deform, resulting in changes in their original volume and shape. Within the limits of linear elasticity, the ratio between the relative deformation in the transverse direction ($\Delta T/T = \varepsilon_t$) and in that taking place in the longitudinal direction ($\Delta L/L = \varepsilon_l$) during a longitudinal uniaxial loading is a constant expressed by $\nu = -\varepsilon_t/\varepsilon_l$, the Poisson's ratio. Depending on the loading nature (tension or compression), one of the terms will be negative, resulting in a positive value for most isotropic materials within $0 \leq \nu \leq ½$. Compliant behaviors are characteristic of incompressible materials, exhibiting a large volume change when loaded, determined by the Bulk modulus B, typical for materials with high atomic density. Less dense materials are usually more compressible, undergoing shape changes more easily than volume changes, a behavior determined by the shear modulus G. The relationship between these three constants is expressed by:

$$\nu = (3B - 2G)/(2G + 6B) \quad (1)$$

This relation sets the maximum limit of ν at ½ for materials with $B \gg G$, that is, $B/G \gg 1$, being rubber a classical example. Polymers in general tend to $\nu > 0.3$, while ceramics lay between 0.25–0.3 and glasses slightly lower, in the range of 0.15–0.3 [22,23]. Some materials may exhibit contraction or expansion in both directions when loaded uniaxially, showing negative Poisson's ratios (i.e., $\nu \to -1$), meaning that B/G approaches 0. This behavior has little relation to the material's atomic arrangement per se, but are rather common for materials with network-like configurations with cellular structures exhibiting folding or rotational capabilities [22]. Performing laborious measurements for each individual elastic constant is generally not necessary, since they are, for isotropic materials, all interrelated:

$$E = 2G(1 + \nu) = 3B(1 - 2\nu). \quad (2)$$

Beside static test methods (tension, compression, bending), three main dynamic measurement methods are widely used: The Resonant Beam Technique (RBT) uses freely suspended beams, which are subjected to vibrations to measure a set of resonance frequencies [24]. The evaluation is based on the solution of the frequency equation from Timoshenko's beam theory. Higher modes are increasingly influenced by shear deformation, which is taken into account by the shear correction factor k. For this factor, analytical expressions are available for isotropic [25] and anisotropic materials [26]. By fitting theoretical to experimental frequencies, Young's and shear modulus are obtained.

Similar to RBT, in Resonant Ultrasound Spectroscopy (RUS) small samples are excited to resonance vibrations [27]. The difference to RBT is that RUS samples usually exhibit a cube- or disc-shaped geometry. The second difference concerns the theory, which is in case of RUS a full description of mechanical vibrations of a solid. This allows the determination of the full elastic tensor from one single measurement [28]. The disadvantage is that the number of resonance frequencies is sometimes very high, which requires pre-knowledge of the sample in order to uniquely attribute experimental to theoretical frequencies.

Ultrasonic Pulse Echo (PE) methods offer a cheap and fast approach to measure elastic constants: The time span between pulse and echo is determined to result in values for quasi-longitudinal and quasi-transverse acoustic wave velocities ("quasi" for the anisotropic case) with respect to different crystal directions. Elastic constants are derived from these velocities [29,30].

We present in the following data for each of these dynamic methods and discuss advantages and limitations of the respective technique.

3. Materials and methods

3.1. Materials and specimen preparation

The evaluated restoratives were selected to encompass materials of different classes and clinical indications (Table 1). Due to its wide range of application and the decreased interest in alumina ceramics in dentistry, a 3 mol% yttria-stabilized tetragonal zirconium dioxide (3Y-TZP) material (e.max ZirCAD) was chosen as the solely representative of glass-free polycrystalline ceramics. The 3Y-TZP powder is combined with a binder and isostatically pressed to form blocks, which are later pre-sintered before machining. The material e.max CAD is delivered in blocks of partially crystallized lithium metasilicate precursory phase, and tinted with bluish pigment. A single or a two-stage heat-treatment (depending on the oven used) of the material follows from that, resulting in needle-shaped lithium disilicate crystals of 2 μm in length randomly orientated embedded in a 30 vol% residual $Li_2O{\cdot}2SiO_2$ glass phase. The materials Suprinity and Celtra Duo

Table 1 – Evaluated materials, their manufacturers, material class and clinical indication.

Material	Manufacturer	Class/terminology	Clinical indication[a]
e.max ZirCAD	Ivoclar-Vivadent	3 mol% Yttria-stabilized tetragonal zirconia polycrystals (3Y-TZP)	Framework for single- and multi-unit (3–12 elements) fixed-partial dentures.
e.max CAD	Ivoclar-Vivadent	Lithium disilicate (LS_2) glass-ceramic	Veneers; inlays; onlays; anterior and posterior crowns; anterior and posterior implant abutments; three-unit bridges up to premolars; overlay veneers for multi-unit frameworks.
Celtra Duo	Dentsply DeTrey	Fully-sintered lithium silicate/phosphate (LSP) glass-ceramic	Veneers; inlays; onlays; anterior and posterior crowns.
Suprinity	VITA Zahnfabrik	Pre-sintered lithium silicate/phosphate (LSP) glass-ceramic	Veneers; inlays; onlays; anterior and posterior crowns.
Vitablocs Mark II	VITA Zahnfabrik	Feldspar-reinforced aluminosilicate glass (FAG)	Veneers; inlays; onlays; anterior and posterior crowns; overlay veneers for multi-unit frameworks.
Empress CAD	Ivoclar-Vivadent	Leucite-based glass-ceramic (LG)	Veneers; inlays; onlays; anterior and posterior crowns.
Enamic	VITA Zahnfabrik	Polymer-infiltrated reinforced-glass network (PIRGN)	Veneers; inlays; onlays; anterior and posterior crowns.
Lava ultimate	3M ESPE	Nano-particulate pre-polymerized resin composite (RC)	Veneers; inlays; onlays.

[a] Clinical indication as given by the manufacturer.

are essentially the same material, developed by both manufacturers in conjunction with the Fraunhofer Institute for Silicate Research (ISC) in Würzburg, Germany. They consist of a lithium silicate glass containing ZrO_2 that uses diphosphorus pentoxide (P_2O_5) as nucleation agent for crystallization of lithium metasilicate. To date the manufacturer of Suprinity supplies the material as a pre-crystallized version that needs to undergo a crystallization firing after machining. The company Dentsply DeTrey in turn, supplies the material in both pre-crystallized (Celtra CAD) and fully crystallized (Celtra Duo) stages as blocks for machining. For our study the pre-crystallized version Suprinity and the fully crystallized version Celtra Duo were selected. Vitablocs Mark II and Empress CAD are well established materials derived from early generations of CAD/CAM blocks, containing feldspar or leucite crystals up to 40 vol% embedded in an aluminosilicate (feldspathic) glass matrix. Enamic is a hybrid material containing a reinforced glass phase (86 wt%, 75 vol%, according to the manufacturer) and a polymeric phase (urethane dimethacrylate and triethylene glycol dimethacrylate). The glassy phase of Enamic is sintered to a porous structure, which is later infiltrated with resin monomers under high pressure. Lava Ultimate is a typical resin composite based on the polymerizable Filtek Supreme Ultra (3M, St. Paul, MN, USA) product, containing dispersed nanometric colloidal silica and ZrO_2 spherical particles in agglomerated and non-agglomerated form (80 wt%, 65 vol%) embedded in a dimethacrylate resin, being industrially pre-polymerized in block form under ideal temperature and pressure conditions.

The respective CAD/CAM blocks were sectioned using a precision cutting machine (Buehler, USA) and a diamond-embedded copper disc under water irrigation. For the measurement of elastic constants, two specimen geometries were used: a parallelepiped (14 mm × 12 mm × 10 mm) and a beam (2 mm × 4 mm × 15 mm) (Fig. 1). Parallel walls were ensured by grinding the sides with a diamond wheel in a grind-

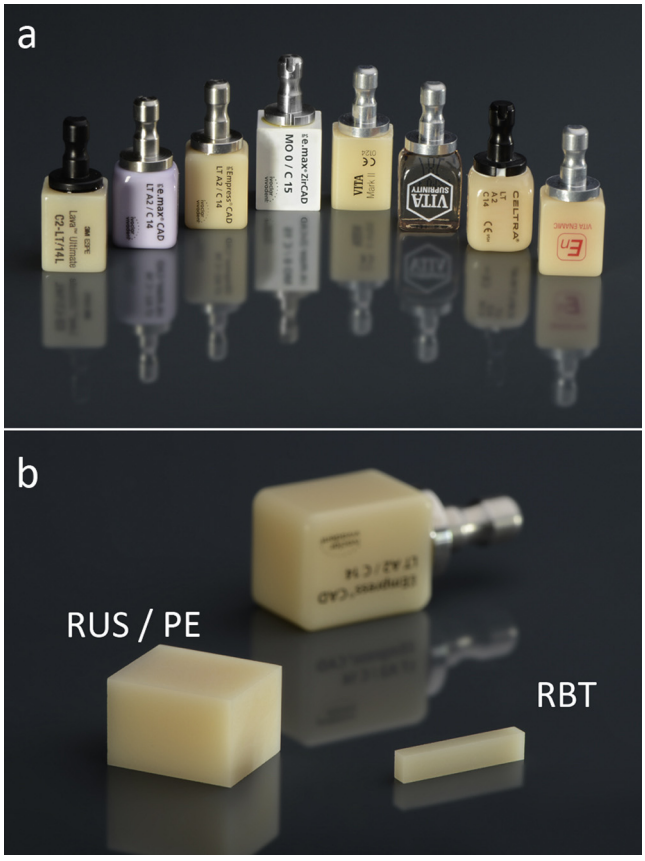

Fig. 1 – (a) Chairside CAD/CAM blocks selected for this study. (b) Specimen sizes and geometries used for the measurements of the elastic constants (RUS = Resonant Ultrasound Spectroscopy, PE = Pulse-echo, RBT = Resonant Beam Technique).

ing machine, up to 0.01 mm toleration. The materials e.max ZirCAD was sintered at 1550 °C for 2 h and cooled overnight. The materials e.max.CAD and Suprinity were crystallized according to the manufacturers instructions in a Vacumat 4000 oven (Vita Zahnfabrik). All other materials were not further treated.

3.2. Measurement of elastic properties

For RBT, prismatic samples were carefully machined to the dimension 15 × 4 × 2 mm^3. The beams were suspended in alumina fiber loops attached to piezoelectric transducers. One transducer excites vibrations, the other detects the resonance answer of the sample. Signal processing is performed with the aid of a network analyzer (HP 8751A) with a signal to noise ratio of up to −140 dBm. In extension of the European standard EN-15335:2007 [31] not only bending, but also torsional vibrations were used for evaluation. For RUS, nearly cuboid samples with an edge length of approximately 10 mm were machined. These samples were placed directly between two piezoelectric transducers. Signal processing is the same as described above, and evaluation is performed according to the literature [27]. For pulse echo measurements, the same samples as for RUS were used and directly contacted with honey. The wave velocities were derived from thickness measurement using an Olympus MG2 equipped with a longitudinal and a torsional transducer (V112-RM and V156-RM). From the longitudinal and transverse wave velocities, Young's and shear modulus were calculated.

3.3. Material characterization

Since the chemical structure and the microstructural features both define the mechanical behavior of materials, a thorough characterization is in order. Samples of all materials were obtained from blocks and prepared for Scanning Electron Microscopy (SEM) and Raman Spectroscopy as described above. Polished (SiC paper, up to 4000 grit in water) and etched specimens (5% Hydrofluoric acid, from 0 to 40 s) were gold sputtered an inserted in a SEM (Auriga, Zeiss, Germany) for microstructural imaging and qualitative Energy Dispersive X-ray Spectroscopy (EDX). To collect their Raman spectra, polished specimens were excited with a 532 nm wavelength Ar^+ laser through a 50× objective with a 100 μm pinhole aperture in 6 successive measurements of 60 s integration time each (Nicolet Almega XR, Thermo Fischer Scientific, Waltham, USA). Step-scan powder diffraction data were recorded using a Siemens D500 diffractometer (Siemens AG, Munich, Germany) with a Cu X-ray tube operating at 30 kV and 30 mA. The spectra were recorded in the 2-theta range from 5° to 70° with a 0.02° step and 1 s counting time. For e.max ZirCAD the powder was obtained from pulverizing the pre-sintered block.

4. Results

4.1. Elastic constants

Depending on the material tested the methods used to measure the elastic constants agreed well or showed significant differences. The results are summarized in Table 2. Apart from

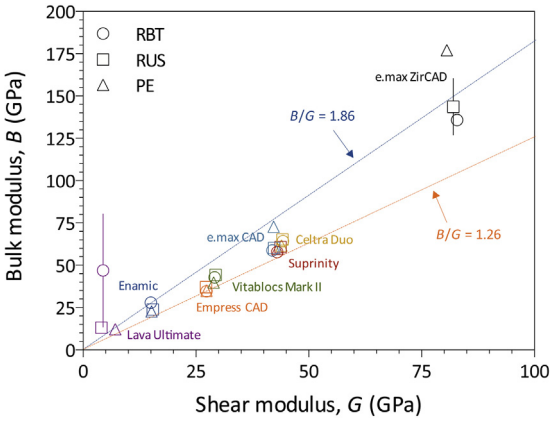

Fig. 2 – Plot Bulk modulus vs. Shear modulus showing the data points for the eight materials measured with RUS, RBT and PE methods.

the hybrid materials (Enamic and Lava Ultimate), RBT and RUS methods showed a good agreement within measurement errors. For these methods the Poisson's ratio of dental ceramics fell within the range $0.20 < \nu < 0.25$, with upper and lower B/G bounds of 1.86 and 1.26, respectively, set by Enamic and Empress CAD (Fig. 2). Compared to RBT and RUS, PE tended to overestimate ν values for e.max ZirCAD and e.max CAD, while underestimating it for Vitablocs Mark II. For the glass-ceramics Suprinity, Celtra Duo and Empress CAD all methods seemed in accord. For Lava Ultimate the damping behavior of the polymeric portion led to unreliable values for RUS and PE especially. For Enamic this effect was observed to a lesser extent, and lead to an overestimation of ν using the RBT method. See details in Section 5.

4.2. Microstructural and phase characterization

SEM images of the investigated materials are illustrated in Figs. 3 and 4 at low and high magnifications. To bring out contrast between phases most materials were etched with 5% Hydrofluoric acid (HF), with exception of e.max ZirCAD. Materials containing finer microstructure, such as Celtra Duo and Suprinity, a highly diluted solution of 0.5% HF was used.

The e.max ZirCAD material showed a polycrystalline-grained structure having no glassy phase and narrow grain size distribution in the order of 0.2–1 μm. The LS_2 glass-ceramic e.max CAD showed an interlocked microstructure composed exclusively of randomly oriented $Li_2Si_2O_5$ crystals of low aspect ratio with their c-axis between 1–2 μm, revealed by the partial dissolution of the surrounding lithium disilicate glass. Expectedly, the materials Celtra Duo and Suprinity showed very similar microstructures, constituted of mainly two crystal phases. The larger, submicrometric crystallites are lithium metasilicates (Li_2SO_3) having round and slightly elongated shapes, with lithium orthophosphates (Li_3PO_4) appearing as round diminute granules of nanometric size. A marked difference between Celtra Duo and Suprinity is the size of the Li_2SO_3 phase, which appears to have grown larger in Celtra Duo (up to ~1 μm in length) than in Suprinity (~0.5 μm). Vitablocs Mark II revealed one glassy phase embed-

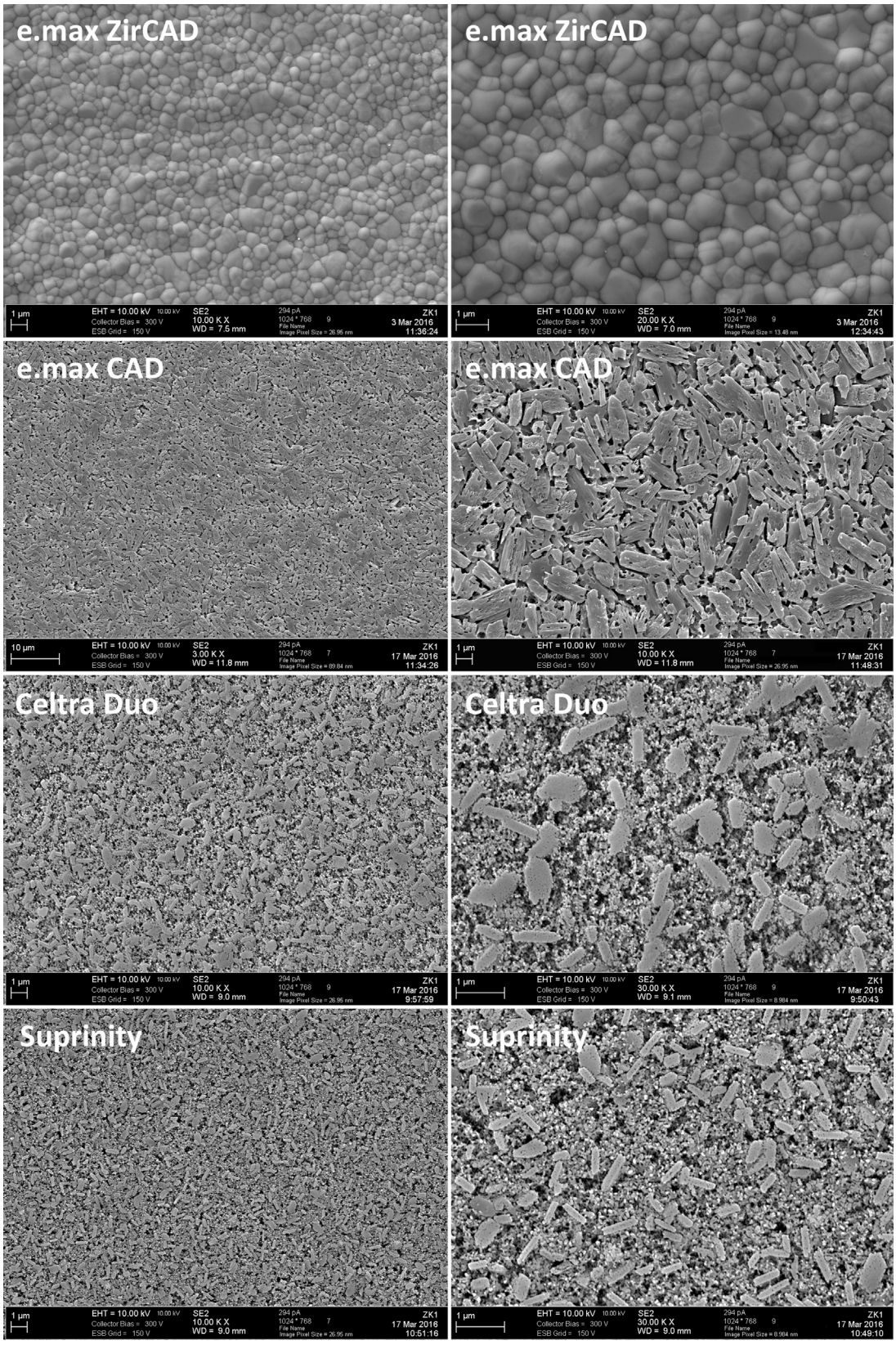

Fig. 3 – SEM images in two magnifications (side by side) of the microstructure of four of the evaluated materials. E.max ZirCAD was polished before final sintering. The fully crystallized glass-ceramics were polished and etched with HF acid (5% for e.max CAD and 0.5% for Suprinity and Celtra Duo).

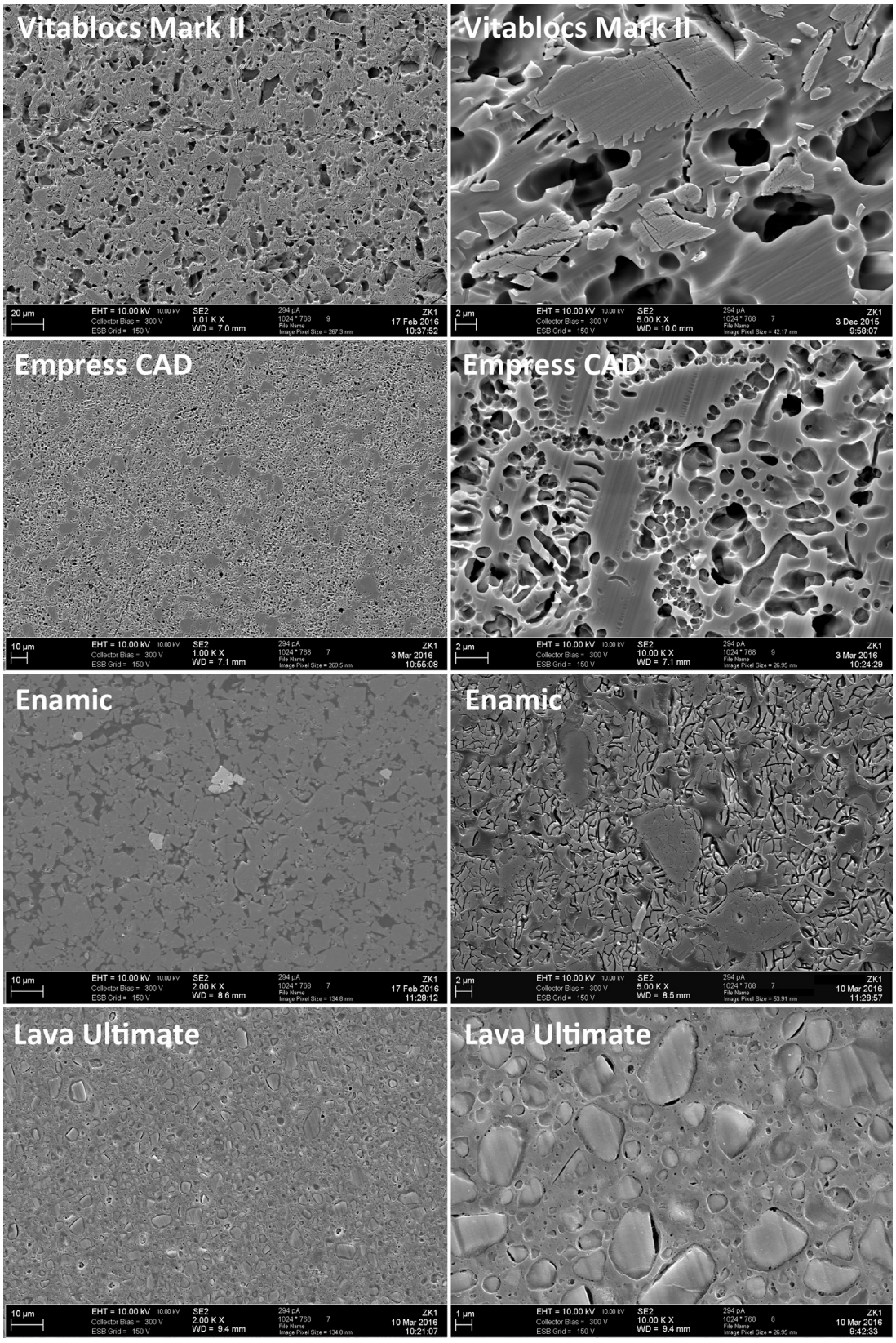

Fig. 4 – SEM images in two magnifications (side by side) of the microstructure of four of the evaluated materials. All materials were polished and etched with 5% HF acid. The low magnification of Enamic was left unetched for clear visualization of the contrasting organic and inorganic phases.

Table 2 – Density and elastic constants obtained using RBT, RUS and PE methods.

		ρ (g/cm^3)	E (GPa)	G (GPa)	B (GPa)	ν
E.max ZirCAD	RBT #1	5.970 ± 0.041	206.3 ± 3.4	82.9 ± 1.4	134.3	0.244 ± 0.03
	RBT #2	5.981 ± 0.041	207.1 ± 3.6	82.9 ± 1.5	137.5	0.249 ± 0.03
	RUS #1	6.059	204.1	82.2	131.8	0.242
	RUS #2	6.051	208.9	81.9	155.4	0.276
	PE #1	–	210.4	80.6	178.9	0.304
	PE #2	–	210.3	80.9	175.2	0.300
E.max CAD	RBT #1	2.466 ± 0.017	102.5 ± 1.6	42.2 ± 0.7	60.1	0.216 ± 0.01
	RBT #2	2.441 ± 0.017	100.7 ± 1.4	41.7 ± 0.6	57.4	0.208 ± 0.01
	RUS #1	2.472	102.8	42.3	59.9	0.214
	RUS #2	2.468	103.1	42.4	60.5	0.216
	PE #1	–	105.1	41.7	72.9	0.260
	PE #2	–	107.0	42.7	72.5	0.254
Celtra Duo	RBT #1	2.623 ± 0.019	107.6 ± 1.6	44.1 ± 0.7	64.0	0.220 ± 0.01
	RBT #2	2.627 ± 0.019	108.6 ± 1.6	44.5 ± 0.7	64.6	0.220 ± 0.01
	RUS #1	2.630	108.2	44.2	65.3	0.224
	RUS #2	2.624	108.2	44.2	65.3	0.224
	PE #1	–	106.6	44.1	61.0	0.209
	PE #2	–	106.5	43.8	62.2	0.215
Suprinity	RBT #1	2.604 ± 0.018	102.9 ± 1.5	43.0 ± 0.7	56.2	0.195 ± 0.01
	RBT #2	2.574 ± 0.018	103.9 ± 1.5	43.0 ± 0.7	59.3	0.208 ± 0.01
	RUS #1	2.643	105.8	43.8	60.2	0.207
	RUS #2	2.641	106.0	43.7	61.3	0.212
	PE #1	–	103.4	42.8	59.0	0.208
	PE #2	–	104.7	43.3	60.1	0.210
Vitablocs Mark II	RBT #1	2.424 ± 0.017	70.1 ± 1.0	28.4 ± 0.5	43.5	0.232 ± 0.01
	RBT #2	2.45 ± 0.018	72.2 ± 1.1	29.9 ± 0.5	42.2	0.215 ± 0.01
	RUS #1	2.461	72.4	29.4	44.7	0.230
	RUS #2	2.460	71.8	29.3	43.7	0.226
	PE #1	–	69.6	28.8	39.6	0.207
	PE #2	–	70.3	29.1	40.0	0.207
Empress CAD	RBT #1	2.434 ± 0.017	65.3 ± 0.64	27.2 ± 0.6	36.4	0.201 ± 0.01
	RBT #2		64.4 ± 0.5	27.5 ± 0.4	32.8	0.173 ± 0.01
	RUS #1	2.438	65.8	27.3	37.4	0.207
	RUS #2		65.6	27.2	36.8	0.203
	PE #1	–	65.5	27.5	35.3	0.191
	PE #2	–	64.7	27.2	34.5	0.188
Enamic	RBT #1	2.128 ± 0.015	37.4 ± 0.6	15.4 ± 0.3	25.9	0.260 ± 0.01
	RBT #2	2.130 ± 0.015	37.6 ± 0.6	14.6 ± 0.03	29.8	0.290 ± 0.01
	RUS #1	2.142	38.11	15.33	24.7	0.243
	RUS #2	2.146	38.05	15.57	22.8	0.222
	PE #1	–	37.3	15.3	22.2	0.220
	PE #2	–	37.0	15.0	23.0	0.232
Lava Ultimate	RBT #1	1.968 ± 0.028	12.7 ± 0.3	4.3 ± 0.3	70.5	0.47 ± 0.05
	RBT #2	1.959 ± 0.028	12.6 ± 0.3	4.5 ± 0.3	23.3	0.41 ± 0.05
	RUS #1	1.977	11.05	4.04	13.9	0.368
	RUS #2	1.975	10.9	4.02	12.3	0.353
	PE #1	–	17.9	7.1	12.3	0.258
	PE #2	–	17.8	7.1	12.2	0.258

Refers to the specimen number. For RUS and PE the same specimens were used for both measurements.

ding two distinguished particulate phases, both reaching up to 15 μm in size: a highly etchable glass and an acid-resistant crystal. The etching pattern in Vitablocs Mark II is due to the dissolution of the high-fusion glass particles by the HF etchant, while the low-fusion glassy matrix is more acid resistant. Etching of Empress CAD resulted in well-dispersed round and slightly elongated cavities in the range of 0.5–3 μm, the shape and size of dissolved crystallites. Enamic has shown two distinct interpenetrating phases with sporadic particles of a third and fourth phase. When etched, the glassy phase is partially dissolved revealing crystalline particles (up to ~20 μm) and exposing the boundaries of the acid-resistant polymeric network. The particulate-reinforced resin composite Lava Ultimate was also etched to render a better contrast between particles and polymer matrix. Irregular particles or particle agglomerates ranging from submicrometric up to 10 μm can

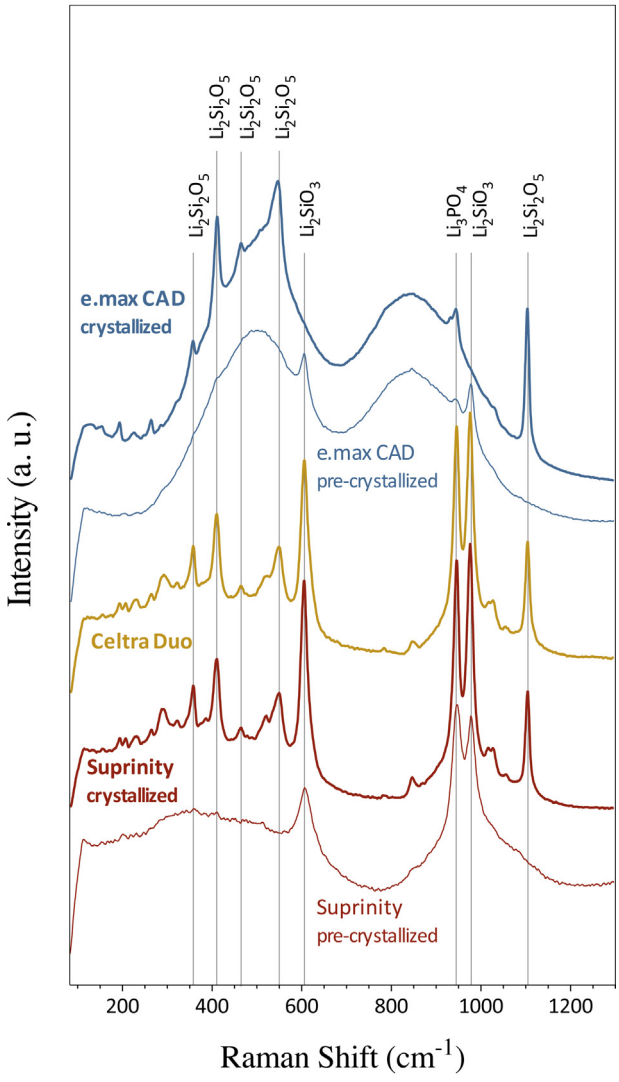

Fig. 5 – Raman spectra of e.max CAD, Suprinity and Celtra Duo. The evolution of the microstructure in e.max CAD and Suprinity is illustrated by the spectra of the uncrystallized and crystallized specimens.

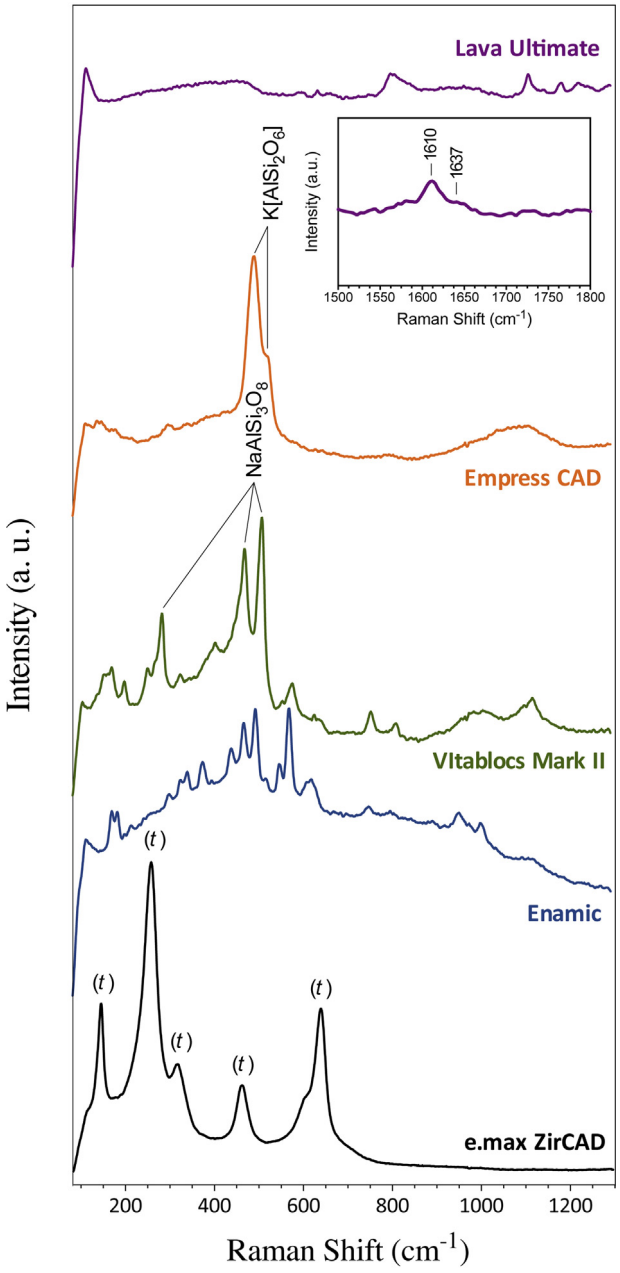

Fig. 6 – Raman spectra of e.max ZirCAD, Enamic, Vitablocs Mark II, Empress CAD and Lava Ultimate.

be seen, with regions around particles being especially susceptible to acid attack.

Raman spectra of e.max CAD and Suprinity in pre-crystallized and crystallized state are shown in Fig. 5, along with the Raman spectra of Celtra Duo. As expected, crystallized Suprinity and Celtra Duo show the same composition, with matching Raman spectra. The glassy pre-crystallized state of Suprinity (and Celtra Duo, consequently) showed three main peaks, respectively related to a lithium metasilicate Li_2SiO_3 (605 cm^{-1} and 976 cm^{-1}) and a lithium orthophosphate Li_3PO_4 (single peak at 946 cm^{-1}) crystal phases. After crystallization firing a significant increase in intensity was observed for these two phases, and a new crystal phase appears, lithium disilicate $Li_2Si_2O_5$, with low bands at 356 cm^{-1} and 464 cm^{-1}, and main bands at 410 cm^{-1}, 546 cm^{-1} and 1106 cm^{-1}. The peaks for the advertised ZrO_2 dispersed in the glass matrix could not be identified due to low concentration and peaks overlapping those of the Li-phases. However, zirconium was detected by EDX in Suprinity (Fig. 7) and Celtra Duo, suggesting its presence dissolved in the glassy phase instead of as reinforcing particle. The lithium disilicate glass of e.max CAD (not-fired) showed two weak bands corresponding to Li_2SiO_3 and a faint peak at 946 cm^{-1} for Li_3PO_4. After crystallization firing the Li_2SiO_3 disappeared and a dominant lithium disilicate crystalline phase became visible. A secondary crystals phase corresponding to Li_3PO_4 persisted, showing a higher intensity compared to the pre-crystallized state.

Raman spectra of e.max ZirCAD, Enamic, Vitablocs Mark II, Empress CAD and Lava Ultimate are depicted in Fig. 6. The sintered e.max ZirCAD showed only peaks related to tetragonal zirconia, which were not seen in Enamic nor in Vitablocks

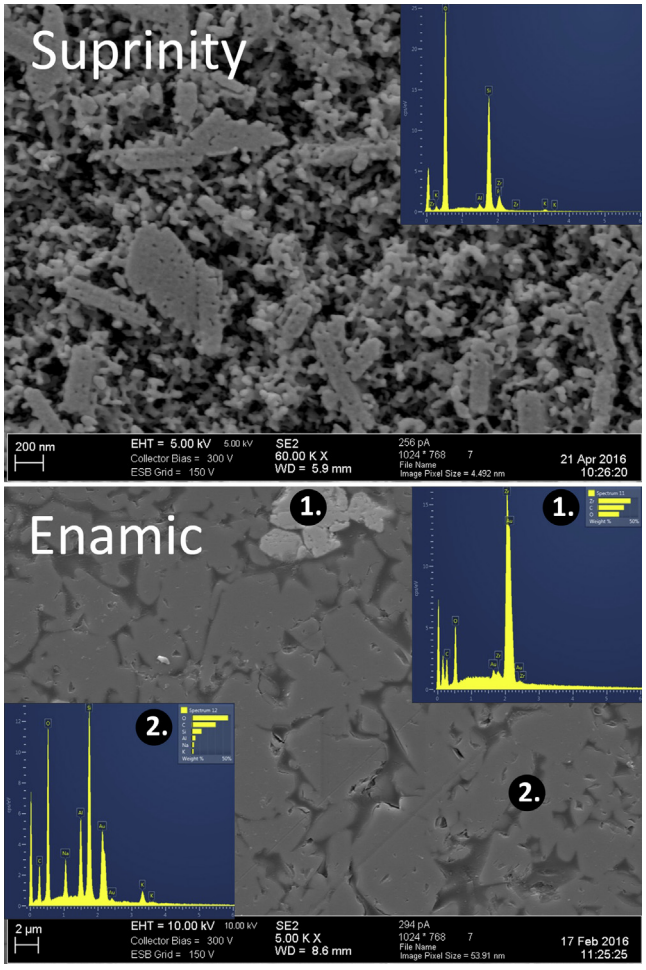

Fig. 7 – EDX point-measurements on unsputtered Suprinity showing the presence of the Zr element in the glass, and two point-measurements on gold-sputtered Enamic showing the Zirconia particle in point 1 and a higher amount of C and O elements from the organic phase in point 2.

Mark II, even though dispersed zirconia particles have been identified in their microstructure by EDX (shown for Enamic in Fig. 7). The crystalline spectrum of Enamic resembles those of feldspars, but did not match any particular mineral. Vitablocs Mark II, in turn, showed main peaks matching those of albite ($NaAlSi_3O_8$) at 285 cm^{-1}, 471 cm^{-1} and 510 cm^{-1}; and Empress CAD those of leucite ($K[AlSi_2O_6]$) at 492 cm^{-1} and 520 cm^{-1}. For Lava Ultimate no crystal phase was discernable, but a high monomer conversion was confirmed following from the flattening of the aliphatic C=C stretching vibration at 1647 cm^{-1} and increase in the aromatic C···C vibration at 1610 cm^{-1}.

XRD data for the crystallized phases was in agreement with the Raman results for most materials. In Fig. 8 XRD patterns for Suprinity, Celtra Duo and e.max CAD are shown. In the pre-crystallized Suprinity the glassy matrix and the poor-crystallized phases Li_2SiO_3 and Li_3PO_4 are clearly noticeable, whereas after firing the main phase found in crystallized Suprinity is Li_2SiO_3, along with the lithium disilicate $Li_2Si_2O_5$ and lithium orthophosphate Li_3PO_4. Between crystallized

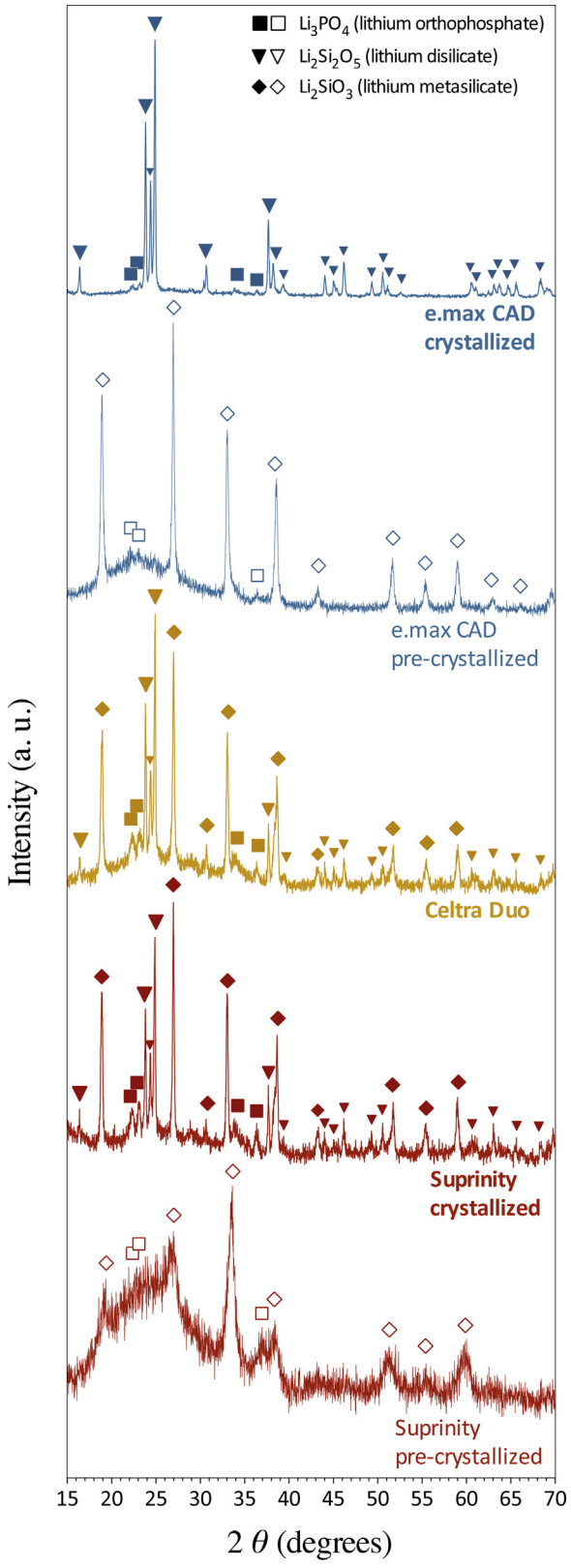

Fig. 8 – XRD patterns of e.max CAD, Suprinity and Celtra Duo. The evolution of the microstructure in e.max CAD and Suprinity is illustrated by the patterns of the uncrystallized and crystallized specimens.

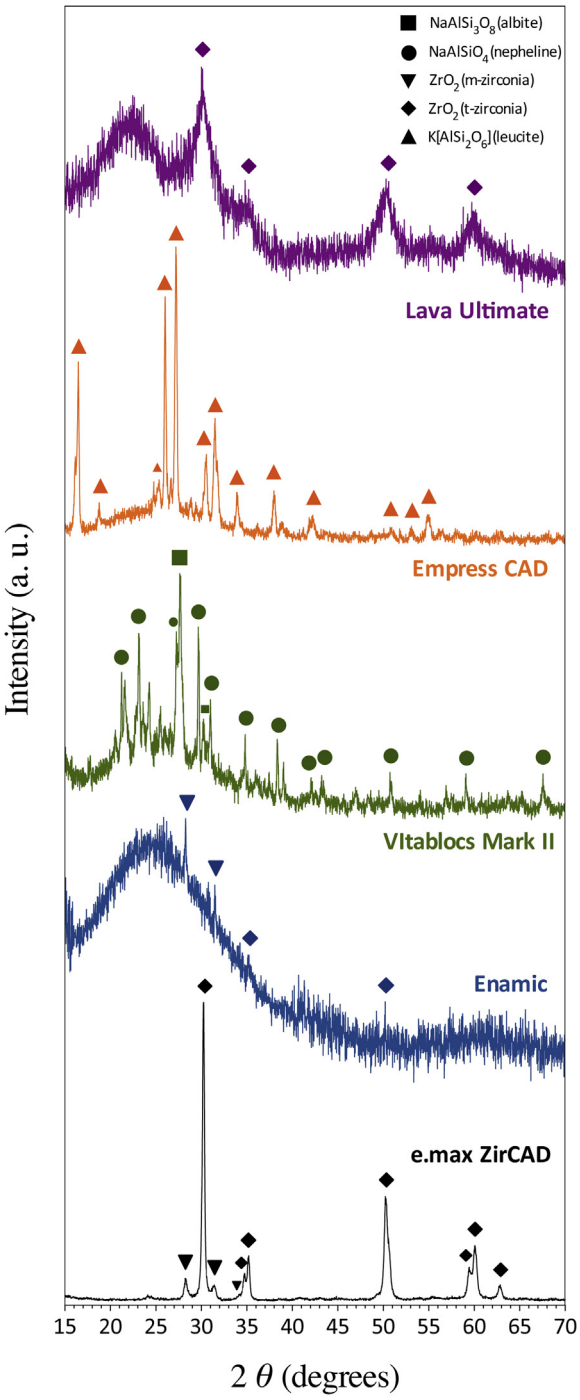

Fig. 9 – XRD patterns of e.max ZirCAD, Enamic, Vitablocs Mark II, Empress CAD and Lava Ultimate.

Suprinity and Celtra Duo the intensity of the $Li_2Si_2O_5$ peaks also differed, being higher for the latter. In e-max CAD the Li_2SiO_3 phase present in the pre-crystallized blocks disappeared completely giving place to a main $Li_2Si_2O_5$ phase and a remaining Li_3PO_4 fraction. In Fig. 9 the XRD patterns of e.max ZirCAD, Enamic, Vitablocs Mark II, Empress CAD and Lava Ultimate are illustrated. In pre-sintered e.max ZirCAD both monoclinic and tetragonal zirconia phases are present, being also the only crystal phases detected in Enamic and Lava Ultimate. The XRD patterns of Vitablocs Mark II match those of nepheline $(Na,K)AlSiO_4$ to a better extent, although albite $(Ca,Na)AlSi_3O_8$ is also detected, though with missing peaks. Leucite $K[AlSi_2O_6]$ was the only phase found in Empress CAD.

5. Discussion

5.1. *Elastic constants*

Most of tested materials exhibit a Poisson's ratio within the range $0.20 < \upsilon < 0.30$ for all three test methods as shown in Table 2. Also, the values for Young's and shear modulus are in very good coincidence for the three measurement techniques, with the exception of Lava Ultimate. A typical error for the moduli in RBT is about 1%, and about 0.5% for RUS. The error depends on the quality of the resonance signal and the number of uniquely identified resonance frequencies. A main cause of error is the quality of sample preparation: The sample dimensions should be prepared to 0.01 mm precision by avoiding any trapezoidal cross section. The higher error for RBT in comparison to RUS results in our case from the smaller lateral dimensions of the RBT samples (about 3 mm in comparison to 10 mm for RUS). An error of 1% in the moduli leads to an error of more than 8% in Poisson's ratio by using Gaussian error propagation. Therefore, a difference in Poisson's ratio of less than about 10% in Table 2 is seen as insignificant. Taking this into account, all measured values for Poisson's ratio by RBT and RUS are identical, with the exception of Lava Ultimate. For the PE technique, a higher value for Poisson's ratio is observed for the zirconia ceramics e.max ZirCAD and the glass ceramics e.max CAD, whereas it is lower for the Feldspar-reinforced aluminosilicate glass Vitablocs Mark II, and probably for both samples with strong polymeric content (Enamic and Lava Ultimate). For the glass-ceramics, Poisson's ratio coincides for all test methods. It is also consistent with literature data of purely amorphous glasses for dental applications (e.g. alkali-, boro-aluminosilicate or lithium disilicate glasses: υ of 0.223, 0.224 and 0.230, respectively) [41,42]. Partial crystallization of glasses tends to lead to an increase in υ, as measured for lithium disilicates, from 0.23 for the base glass to 0.24 for a glass-ceramic with 0.25 aspect ratio $Li_2Si_2O_5$ crystals (similar to e.max CAD), up to $\upsilon = 0.26$ for a LS_2 glass-ceramic with longer crystals of 0.125 aspect ratio (IPS Empress 2, Ivoclar-Vivadent) [41]. For a number of dental materials, higher values for Poisson's ratio are reported in the literature, i.e. Poisson's ratio of the pressable version of Empress CAD (i.e., IPS Empress) was measured to 0.27 [43], or 3Y-TZP having $\upsilon = 0.32$ [44]. This is in coincidence with our observation of differences between the techniques, and is not surprising as dental literature makes wide use of the PE technique. The method is based on ASTM E494 standard [45], which uses longitudinal and transverse wave velocities to calculate elastic constants. Differently to RBT and RUS, which are based on free vibrations of samples at very low strains, PE techniques require the use of a coupling agent and a higher strain. This can have an influence on the measured velocities. Additionally, the reflected wave front may have some interaction with the sample boundaries, which could lead to a distortion. A distortion and dispersion of the wavefront could also be caused by a specific texture

of the sample, such as a needle-like shaped second phase within the material, which hampers the precise determination of the wave velocities. The particular advantage, however, of the PE technique is that it is a very simple and cheap method, whereas the other methods require more experience and a higher effort in evaluation. The advantage of RUS is that it is very accurate and able to measure the complete elastic tensor of anisotropic materials [46], whereas the advantage of RBT is that resonance frequencies are more easily identified and the method can be extended to porous and anisotropic materials at extremely high temperatures [47]. Thus, each of the techniques has its specific merits and limitations.

The dental materials with a high polymeric content (Enamic and Lava Ultimate) should be considered separately: Damping is considerably increased in polymers, which is unfavorable for all dynamic techniques. For RBT and RUS, this leads to a broadening or even disappearance of resonance peaks, which at least requires many measurements of the same sample to ensure that the correct set of resonances was identified. For PE, the pulse may be too weak and distorted so that no reliable values for the wave velocities are obtained. Nevertheless, for Enamic there is a good coincidence for moduli and Poisson's ratio. Differently, for Lava Ultimate significantly higher values for Young's and shear modulus were obtained with PE, which are not seen as reliable. Due to peak broadening, also RBT and RUS deliver values, that differ considerably and are thus not without doubt.

Values for Poisson's ratio for modern particulate-filled dental resin composites are reported in the literature between 0.30 and 0.39 (measured in tension) [48], up to 0.44 (measured in compression) [49]. For the light-cured precursor of Lava Ultimate (Filtek Supreme XT, 3M ESPE), Masouras et al. [50] measured a υ of 0.45, at the upper bound of our value for Lava Ultimate obtained using RBT. Our values for Poisson's ratio fall in this range. A strong difference between tension and compression might lead to ambiguities for Poisson's ratio obtained from different measurement techniques. More accurate ways to determine elastic properties of dental resin composites require the use of a mix of static and dynamic methods. This should help to control the influence of the strong signal damping, which arises from the polymer part of the samples, and to exclude effects from a strong non-linearity of the stress strain curve, which is problematic in static test methods.

According to the manufacturers, Enamic and Lava Ultimate exhibit a comparable overall ceramic/polymer ratio: 86/14 mass% in Enamic and 80/20 mass% in Lava Ultimate. Lava Ultimate contains next to common silica fillers a considerable amount of zirconia nanofillers that increase the overall density and lead to a volume filler loading of 65 vol% (Enamic: 75 vol% inorganic phase). The elastic constants however, differ widely from each other. Enamic shows an Young's modulus approximately three-fold higher compared to Lava Ultimate. This is due to the difference in the internal structure of the two composites. While the former is build-up by resin infiltration of a porous ceramic scaffold, the latter consists of differently sized ceramic (nano-) particles mixed to a resin matrix (see Fig. 3). A continuous interpenetrating inorganic phase is responsible for the stiffening of the material in Enamic, while particle (and especially nanoparticle) compounding of ceramic fillers in a resin matrix depends strongly on steric interactions between particles, exhibiting a percolation limit for reinforcement. As consequence – although having similar compositions – a much lower Young's modulus is seen for Lava Ultimate, as the polymer is the continuous phase. The elastic constants are thus governed mainly by the properties of the matrix phase, therefore the strong damping effect interfering with dynamic measurements, especially for Lava Ultimate. For infiltrated ceramic scaffolds such as Enamic, estimations of the elastic modulus based on the properties of the constituents have been attempted [51], which might be of limited applicability for resin composites.

5.2. *Microstructural and phase characterization*

Raman Spectroscopy and X-ray Diffractometry are complementary tools in the compositional characterization of glasses and ceramics. The former renders vibration modes of interatomic bonds from both amorphous and non-amorphous phases, while the latter yields Bragg diffraction angles and distances of lattice planes in crystals. These are fingerprints that can be used to identify unknown crystal structures in a material. For most restoratives analyzed here both methods agreed well on the crystalline phase. Somewhat conversely, for Vitablocs Mark II, while Raman bands indicated the presence of albite $(Ca,Na)AlSi_3O_8$, the diffraction pattern indicated the presence of nepheline $(Na,K)AlSiO_4$. Both minerals are tectosilicates: a Paglioclase of the Feldspar family and a silica-unsaturated feldspathoid. Albite has been identified by the manufacturer as being the main phase in Vitablocs Mark II, in a content below 20 wt% [32]. The irregular borders of the crystallites seen in the SEM micrographs (Fig. 3) of Vitablocs Mark II indicate that they stemmed from natural minerals that were pulverized for use as particle reinforcement of the glass. Crystallites that nucleate from the base glasses and later crystallize under thermal treatment show more homogeneous crystal size distributions and smoother boundaries to the surrounding glass phase, as seen for example for Celtra Duo, Suprinity and Empress CAD. This latter derives from the first formulations of pressable ingots (IPS Empress, Ivoclar-Vivadent) and monolithic blocks for CAD/CAM machining (ProCAD, Ivoclar-Vivadent), that use a SiO_2-Al_2O_3-K_2O-Na_2O glass system for the nucleation and crystallization of leucite crystals [33]. Leucite grows dendritically through surface crystallization of glass particles in powdered glass or by bulk crystallization of monolithic glasses, having TiO_2 and CeO_2 as nucleating agents [34]. The crystalline phase of Enamic remains partially unresolved, as Raman showed both feldspar-like $(Ca,Na)AlSi_3O_8$ features, and small peaks that seem to match with the monoclinic phase of zirconia (m-ZrO_2). XRD shows the broad band of the glassy matrix, and only few zirconia peaks could be observed. The huge organic/inorganic amorphous fraction in Enamic is made visible in both Raman and XRD through the bulging of the patterns, making difficult the identification of the crystalline phases. Similarly, only low-intensity zirconia peaks were detected by XRD for Lava Ultimate, belonging to the zirconia nanoparticles, and evidence of high double bond conversion in the polymer phase through the 1610 cm^{-1} and 1637 cm^{-1} Raman bands.

An insight was gained regarding the microstructure evolution of Suprinity and e.max CAD by analyzing the

pre-crystallized and the post-crystallization stages of both glass-ceramics. The crystallization of Suprinity increased the peak intensity of both Li_3PO_4 and Li_2SiO_3, observed by Raman Spectroscopy and XRD, suggesting an increase in crystal growth and fraction through thermal treatment. Lithium orthophosphate crystallizes rapidly in lithium disilicate glasses containing the nucleating agent P_2O_5 at temperatures as low as 476 °C, according to Iqbal et al. [35]:

$$6(Si–O^{-}\ ^{+}Li)+ P_2O_5 \leftrightarrow 3(Si–O–Si)+ 2Li_3PO_4. \quad (3)$$

The newly formed lithium disilicate phase detected in crystallized Suprinity and Celtra Duo is of relative low intensity when compared to the $Li_2Si_2O_5$ intensity in e.max CAD, and not readily distinguishable from the submicrometric Li_3PO_4 granules in the SEM. The difference in size of the lithium metasilicate crystals between Suprinity and Celtra Duo is seen in the XRD patterns, and may reflect differences in thermal treatment parameters (i.e., time, temperature), since Celtra Duo is supplied ready-to-use (that is, fully sintered in an industrial environment), while Suprinity must undergo a shorter crystallization firing for feasible chairside applications.

The evolution of the crystalline phases in e.max CAD follows the descriptions of Höland et al. [36] for multicomponent lithium disilicate glass systems containing P_2O_5 as nucleation agent and controlled bulk crystallization of $Li_2Si_2O_5$. Lithium metasilicates, the predominant phase in the pre-crystallized blocks, have a lower activation energy and form at lower temperatures (550–750 °C), following:

$$Li_2O\ (glass)+ Q^2\ (glass) = Li_2SiO_3\ (crystal) \quad (5)$$

$$Li_2O\ (glass)+ Q^3\ (glass) = Li_2SiO_3\ (crystal)+ Q^4\ (glass), \quad (6)$$

and serve to partially strengthen the blocks for machining and as precursor for the posterior crystallization of the lithium disilicate crystals. The phases we found in pre- and crystallized e.max CAD agree well with the X-ray Diffraction patterns observed by Lien et al. [37] at different temperature ranges, in which lithium metasilicates were shown to dissolve completely above 780 °C, and lithium disilicates crystallized up to 840 °C. The absence of $Li_2Si_2O_5$ in the pre-crystallized e.max CAD points to a heat treatment below 730 °C, the point where transformation from Li_2SiO_3 to $Li_2Si_2O_5$ begins [36–38], as:

$$Li_2SiO_3\ (crystal)+ Q^4\ (glass) = Li_2Si_2O_5\ (crystal), \quad (7)$$

leading to the disappearance of the lithium metasilicate peak after the crystallization firing. The faint Li_3PO_4 peak in the pre-crystallized block suggests its form as a primary poorly crystalllized phase formed at around 620–730 °C [39], analogously to Eq. (3):

$$P_2O_5\ (glass)+ 3Li_2O\ (glass) = 2Li_3PO_4\ (crystal) \quad (8)$$

which continue to maturate up to 860 °C, resulting in the increased intensity observed in the Raman spectra and XRD pattern in the fully crystallized e.max CAD. Cristobalite, found by Lien et al. [37] after crystallization firing of e.max CAD, and said to provide a further mechanism for the precipitation of $Li_2Si_2O_5$ for compositions having >3 mol% of the nucleating agent P_2O_5 [40], was not observed in our samples. Since measurements at interrupted temperature intervals during crystallization were not conducted, the full consumption of cristobalite may have occurred according to:

$$SiO_2\ (crystal)+ Li_2SiO_3\ (crystal) = Li_2Si_2O_5\ (crystal). \quad (8)$$

To determine that further analyses would be required.

At this point the use of some terminology is in place when referring to the evaluated restorative materials. This can be a barrier, since terms used by manufacturers have a strong focus on commercial appeal and get thereby popularized. Enamic, for example, is advertised as being a "Polymer-Infiltrated Ceramic Network" (PICN), although we have seen here that the inorganic phase is composed mostly of pure glass, with a very low fraction of particle reinforcement. Lava Ultimate is marketed as "Resin Nano-Ceramic", and is nothing but a resin composite containing nano-sized zirconia fillers. Celtra Duo and Suprinity are commercialized as "Zirconia-reinforced Lithium Silicate", although no crystalline zirconia has been detected. It is the opinion of the authors that the coining of material terminology should be based on composition, microstructure and manufacturing process, a task better suited to the scientific community. In Table 1 a terminology for the materials herein evaluated is proposed.

6. Conclusions

The measurement of elastic properties depends on the accuracy of the method employed. For ceramic materials dynamic methods such as Resonant Ultrasound Spectroscopy and Resonant Beam Technique give appropriate results but require theoretical experience and fancy equipment. The Pulse-Echo method is fast and cheap, but falls short in accuracy. For materials containing considerable polymeric fraction, all tested methods show important limitations.

The terminology used to designate new dental materials should be based on the microstructural composition, evaluated through methods such as Raman Spectroscopy and X-ray Diffraction, rather than motivated by marketing appeal.

Aknowledgment

The materials herein tested were kindly donated by the manufacturers.

REFERENCES

[1] ENV 843-1. Monolitische Keramik Mechanische Eigenschaften bei Raumtemperatur. Teil 1: Bestimmung der Bruchzähigkeit; 1995.
[2] ASTM C1161. Standard test method for flexural strength of advanced ceramics at ambient temperature; 2013.
[3] ISO 4049:2009. Dentistry — polymer-based restorative materials; 2010.

[4] ASTM C-1421-99. Test methods for fracture toughness of advanced ceramics; 2002.
[5] ISO 13586. Plastics — determination of fracture toughness (GIc and KIc) — linear elastic fracture mechanics (LEFM) approach; 2000.
[6] EN 14425:3. Advanced technical ceramics — test method for determination of fracture toughness of monolithic ceramics — part 3: chevron notched beam (CNB) method; 2010.
[7] ISO 23146. Fine ceramics (advanced ceramics, advanced technical ceramics) — test methods for fracture toughness of monolithic ceramics — single-edge V-notched beam (SENB) method; 2012.
[8] ISO 24370. Fine ceramics (advanced ceramics, advanced technical ceramics) — test method for fracture toughness of monolithic ceramics at room temperature by chevron-notched beam (CNB) method; 2005.
[9] ISO 6872:2015. Dentistry — ceramic materials; 2015.
[10] Lube T, Manner M, Danzer R. The miniaturization of the 4-point-bend test. Fatigue Fract Eng Mater Struct 1997;30:1605–16.
[11] Pick B, Meira JBC, Driemeier L, Braga RR. A critical view on biaxial and short-beam uniaxial flexural strength tests applied to resin composites using Weibull, fractographic and finite element analysis. Dent Mater 2010;26:83–90.
[12] Lube T, Manner M. Development of a bending-test device for small samples. Key Eng Mater 1997;132–136:488–91.
[13] Börger A, Supancic P, Danzer R. The ball on three balls test for strength testing of brittle discs: stress distributions in the disc. J Eur Ceram Soc 2002;22:1425–36.
[14] Börger A, Supancic P, Danzer R. Strength characterization of small ceramic discs using the ball on three balls test. Ceram Eng Sci Proc 2003;24:365–70.
[15] Börger A, Supancic P, Danzer R. The ball on three balls test for strength testing of brittle discs: part II: analysis of possible errors in the strength determination. J Eur Ceram Soc 2004;24:2917–28.
[16] Börger A, Danzer R, Supancic P. Biaxial strength test of discs of different size using the ball on three balls test. Ceram Eng Sci Proc 2004;25:283–8.
[17] Danzer R. Some notes on the correlation between fracture and defect statistics: are Weibull statistics valid for very small specimens? J Eur Ceram Soc 2006;26:3043–9.
[18] Danzer R, Supancic P, Harrer W. Biaxial tensile strength test for brittle retangular plates. J Ceram Soc Japan 2006;114:1054–60.
[19] Lube T, Rasche S, Nindhia TGT. A fracture toughness test using the ball-on-three-balls test. J Am Ceram Soc 2016;99:249–56.
[20] Strobl S, Rasche S, Krautgasser S, Sharova E, Lube T. Fracture toughness testing of small ceramic discs and plates. J Eur Ceram Soc 2014;34:1637–42.
[21] Strobl S, Supancic P, Lube T, Danzer R. Surface crack in tension or in bending — a reassessment of the Newman and Raju formula in respect to the fracture toughness measurements in brittle materials. J Eur Ceram Soc 2012;32:1491–501.
[22] Greaves GN, Greer AL, Lakes RS, Rouxel T. Poisson's ratio and modern materials. Nat Mater 2011;10:823–37.
[23] Mott PH, Roland CM. Limits to Poisson's ratio in isotropic materials. Phys Rev B 2009;80, 132104-123104-4.
[24] Lins W, Kaindl H, Peterlik H, Kromp A. A novel resonant beam technique to determine the elastic moduli independence on orientation and temperature up to 2000 °C. Rev Sci Instrum 1999;90:3052–8.
[25] Hutchinson JR. Shear coefficients for Timoschenko beam theory. J Appl Mech 2001;68:87–92.
[26] Puchegger S, Loidl D, Kromp K, Peterlik H. Hutchinson's shear coefficients for anisotropic beams. J Sound Vib 2003;266:207–16.
[27] Migliori A, Sarrao JL, Visscher WM, Bell TM, Lei M, Fisk Z, et al. Resonant ultrasound spectroscopy techniques for measurement of the elastic moduli of solids. Physica B 1993;183:1–24.
[28] Leisure RG, Willis FA. Resonant ultrasound spectroscopy. J Phys Condens Matter 1997;9:6001–29.
[29] Papadakis EP. Ultrasonic phase velocity by the Pulse-Echo-Overlap method incorporating diffraction phase corrections. J Acoust Soc Am 1967;42:1045–51.
[30] Sedlak P, Seiner H, Landa M, Novak V, Sittner P, Manosa L. Elastic constants of bbc austenite and 2H osthorombic martensite in CuAlBi shape memory alloy. Acta Mater 2005;53:3643–61.
[31] EN 15335:2007. Advanced technical ceramics — ceramic composites — elastic properties by resonant beam method up to 2000 °C; 2007.
[32] Datzmann G. Cerec vitablocs Mark II machinable ceramic. In: CAD/CAM in aesthetic dentistry: Cerec 10-year aniversary symposium. 1996.
[33] Höland W, Rheinberger V, Apel E, vanít Hoen C. Principles and phenomena of bioengineering with glass-ceramics for dental restoration. J Eur Ceram Soc 2007;27:1521–6.
[34] Höland W, Frank M, Rheinberger V. Surface crystallization of leucite in glasses. J Non-Cryst Solids 1995;180:292–307.
[35] Iqbal Y, Lee WE, Holland D, James PF. Crystal nucleation in P_2O_5-doped lithium disilicate glasses. J Mater Sci 1999;34:4399–411.
[36] Höland W, Apel E, vanít Hoen C, Rheinberger V. Studies of crystal phase formation in high-strength lithium disilicate glass-ceramics. J Non-Cryst Solids 2006;352:4041–50.
[37] Lien W, Roberts HW, Platt JA, Vandewalle KS, Hill TJ, Chu T-MG. Microstructural evolution and physical behavior of a lithium disilicate glass-ceramic. Dent Mater 2015;31:928–40.
[38] Zhang P, Li X, Yang J, Xu S. The crystallization and microstructure evolution of lithium disilicate-based glass-ceramic. J Non-Cryst Solids 2014:392–3.
[39] Huang S, Cao P, Li Y, Huang Z, Gao W. Nucleation and crystallization kinetics of a multicomponent lithium disilicate glass by in situ and real-time synchrotron X-ray diffraction. Cryst Growth Des 2013;13:4031–8.
[40] Wen G, Zheng X, Song L. Effects of P_2O_5 and sintering temperature on microstructure and mechanical properties of lithium disilicate glass-ceramics. Acta Mater 2007;55:3583–91.
[41] Della Bona A, Mecholsky Jr J, Anusavice KJ. Fracture behavior of lithia disilicate and leucite-based ceramics. Dent Mater 2004;20:956–62.
[42] Deubener J, Höland M, Janakiraman N, Rheinberger VM. Crack tip fracture toughness of base glasses for dental restoration glass-ceramics using crack opening displacements. J Mech Behav Biomed Mater 2011;4:1291–8.
[43] Della Bona A, Anusavice KJ, DeHoff PH. Weibull analysis and flexural strength of hot-pressed core and veneered ceramic structures. Dent Mater 2003;19:662–9.
[44] Borba M, de Araújo MD, de Lima E, Yoshimura HN, Cesar PF, Griggs JA, et al. Flexural strength and failure modes of layered ceramic structures. Dent Mater 2011;27:1259–66.
[45] ASTM E494. Standard practice for measuring ultrasonic velocity in materials; 2015.
[46] Bernard S, Grimal Q, Laugier P. Accurate measurement of cortical bone elasticity tensor with resonant ultrasound spectroscopy. J Mech Behav Biomed Mater 2013;18:12–9.
[47] Loidl D, Puchegger S, Kromp K, Zeschky J, Greil P, Bourgeon M, et al. Elastic moduli of porous and anisotropic composites at high temperatures. Adv Eng Mater 2004;6:138–42.

[48] Chung SM, Yap AUJ, Koh WK, Tsai KT, Lim CT. Measurement of Poisson's ratio of dental composite restorative materials. Biomaterials 2004;25:2455–60.
[49] Chabrier F, Lloyd CH, Scrimgeour SN. Measurement at low strain rates of the elastic properties of dental polymeric materials. Dent Mater 1999;15:33–8.
[50] Masouras K, Silikas N, Watts DC. Correlation of filler content and elastic properties of resin-composites. Dent Mater 2008;24:932–9.
[51] Coldea A, Swain MV, Thiel N. Mechanical properties of polymer-infiltrated-ceramic-netwerok materials. Dent Mater 2013;29:419–26.